Shahid Chamran University of Ahvaz

Iranian Association of Electrical and Electronics Engineers

Journal of Applied Research in Electrical Engineering

E-ISSN: 2783-2864
P-ISSN: 2717-414X
Homepage:https://jaree.scu.ac.ir/



Research Article

Optimal Energy Management in Solar-powered Battery-Ultracapacitor Hybrid Electric Vehicles: Leveraging ANN-HDKR for Tilt Angle Optimization

Shraddha Kaushik[1,2*] and Kunamneni Rachanajali[2]

[1]*Department of Electrical Engineering, Bhilai Institute of Technology, Durg, India*

[2]*Department of Electrical & Electronics Engineering, Vignan Foundation for Science Technology & Research, Guntur, India*

** Corresponding Author: shraddha.kaushik@bitdurg.ac.in*

Abstract: This paper presents a comprehensive methodology to improve solar irradiance forecasting and optimize its integration into Hybrid Electric Vehicle (HEV) Energy Management Systems (EMS). Accurate solar irradiance prediction is critical for maximizing renewable energy utilization and ensuring reliable operation of hybrid storage devices. To achieve this, the proposed framework combines Deep Neural Networks (DNNs) with the Horizontal Diffuse K Clearness Index Regression (HDKR) technique for day-ahead forecasting of Global Horizontal Irradiance (GHI). This hybrid approach not only predicts GHI with high precision but also decomposes it into beam, diffuse, and reflected components on tilted surfaces, thereby enabling more realistic modeling of Photovoltaic (PV) generation under varying conditions. The forecasting model achieved an R-squared value of 0.8818 and a Root Mean Square Error (RMSE) of 0.269, confirming its robustness and accuracy. These forecasts are incorporated into a real-time EMS that coordinates energy distribution among the battery, ultracapacitor, and PV subsystems while accounting for seasonal variability, auxiliary system demands, and dynamic driving cycles. Unlike traditional static State of Charge (SOC) targets, the proposed dynamic SOC control adapts to daily, monthly, and seasonal variations, allowing efficient energy sharing between storage devices. This strategy reduces stress on critical battery components by 47.6%, thereby improving both performance and lifespan. Furthermore, the integration of ultracapacitors effectively mitigates transient load demands, ensuring higher system reliability under fluctuating conditions. Overall, the research demonstrates how HDKR-based estimation combined with adaptive EMS strategies can significantly enhance efficiency, sustainability, and durability in solar-assisted HEVs.

Keywords: Solar irradiance forecasting, Energy management scheme, Ultra-Ccapacitor (UC), Photovoltaic (PV), Hybrid Electric Vehicle (HEV).

Article history
Received 22 January 2025; Revised 12 December 2025; Accepted 17 December 2025; Published online 18 January 2026.
© 2026 Published by Shahid Chamran University of Ahvaz & Iranian Association of Electrical and Electronics Engineers (IAEEE)
How to cite this article
S. Kaushik and K. Rachanajali, "Optimal energy management in solar-powered battery-ultracapacitor hybrid electric vehicles: Leveraging ANN-HDKR for tilt angle optimization," *J. Appl. Res. Electr. Eng.*, vol. 4, no. 1, pp. 137-153, 2025. DOI: 10.22055/jaree.2025.48780.1152

Check for updates

NOMENCLATURE

HEV	Hybrid Electric Vehicle
PV	Photovoltaic
LSTM	Long Short-Term Memory
EMS	Energy Management Scheme
UC	Ultra-Capacitor
Solar_Zenith	Solar zenith angle, represents the angle between the direction of the sun and the vertical (zenith) line.
EV	Electric Vehicle
SOC	State Of Charge
MPPT	Maximum Power Point Tracking
P&O	Perturb And observe
ESS	Energy Storage System
ICE	Internal Combustion Engine
HESS	Hybrid Energy Storage System
R^2	Correlation Coefficient
$G_{diffuse,horizontal}$	Diffuse Radiation on the horizontal surface
G_{total}	Total radiation (sum of beam, diffuse and reflected)
R_b	Incidence angle modifier
GHI	Global Horizontal Irradiance

DNI	Direct Normal Irradiance (Beam Radiation)
HESS	Hybrid energy storage system
G_{beam}	Beam radiation on the tilted surface
$G_{beam,\ horizontal}$	Beam radiation on a horizontal surface
G_d	Isotropic Sky Diffuse Radiation
ESS	Energy Storage System
RMSE	Root Mean Square Error
MSE	Mean Square Error
MAE	Mean Absolute Error
RNN	Recurrent Neural Networks
$G_{d,\ \beta}$	Diffuse Radiation on the tilted surface
MPC	Model predictive controller
ML	Machine Learning
Θ	Incidence angle (angle between the normal to the surface and the direction of the sun)
$Θ_{solar}$	Solar Zenith Angle
Kt	Clearness index, representing the ratio of measured solar radiation on a horizontal surface to extraterrestrial solar radiation.

1. INTRODUCTION

1.1. Background

India's transportation sector has set ambitious goals for climate neutrality, aiming to achieve a substantially climate-neutral vehicle stock by 2050. To reach this target, emissions must be reduced by nearly 66% compared to 1990 levels by 2030. In support of this transition, the Indian government introduced policies in 2020 that provided low-interest loans and subsidies of up to 45% for consumers purchasing Hybrid Electric Vehicles (HEVs). These incentives have spurred growth, and by 2023, HEV adoption had increased by 8%, with nearly 10 million units sold nationwide. The majority of these vehicles approximately 76%are compact HEVs primarily used in urban settings. However, fossil fuel-powered vehicles continue to dominate energy consumption, accounting for 70% of personal commuting and 20% of freight transport needs. This ongoing dependence on fossil fuels underscores the urgency of advancing efficient hybrid and electric vehicle technologies. Plug-in Hybrid Electric Vehicles (PHEVs) and Battery Electric Vehicles (BEVs), particularly when powered by renewable energy sources such as solar, are considered essential for reducing greenhouse gas emissions and ensuring sustainable mobility [1]. Projections suggest that by 2030, India's HEV stock could exceed 50 million units, further highlighting the importance of integrating renewable-based energy management solutions. The need for this paper therefore arises from the twin imperatives of decarbonizing transport and exploiting solar resources effectively within HEV architectures.

1.2. Literature Review

Machine Learning (ML) and Deep Learning (DL) approaches have emerged as powerful tools for solar irradiance forecasting, a key enabler of solar-powered HEVs. Techniques such as Recurrent Neural Networks (RNNs), Convolutional Neural Networks (CNNs), Long Short-Term Memory (LSTM) models, and hybrid ensemble methods have been widely studied for their ability to capture nonlinear temporal dependencies in irradiance data [2]. Research has categorized models into residual-based, evolutionary-based, decomposition-based, clustering-based, and hybrid ensemble learning methods, consistently finding that hybrid approaches outperform standalone models, albeit with limited metric-based comparisons [3]. Among these, DL-based LSTM models stand out for their superior forecasting accuracy, often yielding lower Root Mean Square Error (RMSE) values than other methods [4]. Complementary methods such as Random Forest (RF) have also shown promise in estimating Global Horizontal Irradiation (GHI), Beam Normal Irradiation (BNI), and Diffuse Horizontal Irradiation (DHI), with RF outperforming traditional Artificial Neural Networks (ANNs) and smart persistence methods over longer prediction horizons [5].

Solar irradiance estimation on tilted surfaces remains another critical area of research. The Horizontal Diffuse K Clearness Index Regression (HDKR) model has long been used to characterize solar radiation by incorporating tilt angles, atmospheric conditions, and solar positions [6]. Transposition models based on HDKR have been successfully applied for energy system design, though their accuracy is limited by the quality of location-specific input data [7]. Recent works also demonstrate the application of HDKR in diverse domains such as agriculture, architecture, and renewable power generation [8]. Comparative studies of isotropic, anisotropic, and HDKR models confirm HDKR's superior ability to handle tilted surface irradiance estimation [9,10]. These methods are essential in contexts where global and diffuse irradiances are measured, allowing beam irradiance to be derived using $G_h = B_h + D_h$, where G_h, B_h, and D_h represent global, beam, and diffuse irradiances, respectively [10].

Parallelly, the development of Zero-Fuel Zero-Emission (ZFZE) vehicle concepts has inspired hybrid architectures integrating PV, wind energy, fuel cells, and supercapacitors for automotive applications [11]. Such designs leverage in-wheel motors, Proton Exchange Membranes (PEMs), and hybrid storage systems to enhance efficiency and reduce carbon emissions [12]. Energy Management Strategies (EMS) for these systems have been broadly categorized into predictive and non-predictive methods, ranging from rule-based heuristics to model predictive control [13–15]. Despite advancements, most of these methods do not integrate solar forecasting into HEV EMS design.

For instance,[36] proposed a voltage regulation strategy for distribution networks using reactive power from photovoltaic inverters combined with PID consensus algorithms, illustrating the potential of intelligent PV control for improving grid reliability. This [37] paper develops a Deep Neural Network (DNN)-based Nonlinear Model Predictive Control (NMPC) methodology to approximate optimal power management solutions for hybrid electric vehicles. The deep learning model is trained to mimic the outcomes of a computationally intensive NMPC, providing near-optimal energy distribution decisions (e.g., battery vs engine) with significantly reduced computation time, which is essential for real-time scheduling. Together, these works highlight the broader potential of solar energy optimization but reveal that integration with EMS in HEVs remains underexplored.

1.3. Research Gap and Motivation

Although substantial work has been carried out on solar forecasting and EMS design, several gaps remain that motivate this study. First, existing forecasting models focus primarily on horizontal irradiance, with limited attention to tilted-surface predictions crucial for vehicle-mounted PV modules. Second, while HDKR is widely accepted, its dependency on local calibration reduces generalizability across diverse geographies like India. Third, most HEV-EMS frameworks overlook the variability and uncertainty of solar input, failing to dynamically adapt to fluctuating irradiance and driving conditions. Fourth, while battery–ultracapacitor hybrid storage offers complementary benefits, strategies for their optimal real-time coordination under varying load profiles are lacking.

A new method is needed because existing forecasting techniques such as ANNs, Random Forests, or standalone LSTM networks often suffer from overfitting, limited long-horizon accuracy, or lack of adaptability when integrated into real-time EMS. Similarly, conventional EMS approaches, particularly rule-based methods, are simple and computationally efficient but cannot accommodate uncertainties in solar forecasts or seasonal variations, leading to suboptimal energy allocation. Optimization-based EMS, while more advanced, often become computationally expensive and unsuitable for real-time driving conditions. Therefore, integrating a deep learning-based forecasting framework with HDKR for tilted surfaces, and embedding it within a constraint-driven EMS, offers a novel solution that overcomes the limitations of existing models. The motivation for this work is thus to ensure higher prediction accuracy, better adaptability to varying conditions, and improved hybrid storage utilization in solar-assisted HEVs.

1.4. Challenges

The primary challenge this research aims to address is the integration of accurate solar irradiance forecasting with energy management in hybrid electric vehicles (HEVs), where the variability of solar radiation, limitations of conventional ANN-based forecasting models, and inefficiencies in rule-based EMS strategies hinder reliable power distribution between battery and ultracapacitor systems. This work proposes a novel HDKR-based methodology to overcome these challenges by improving solar prediction accuracy on tilted surfaces and developing a constraint-driven EMS for real-time driving conditions.

Despite significant advances in solar forecasting and energy management strategies, several limitations in existing approaches hinder their effectiveness in real-world hybrid electric vehicle (HEV) applications. Traditional solar forecasting methods such as artificial neural networks (ANNs) and Random Forests (RF) provide reasonable short-term accuracy, but their performance often deteriorates for longer horizons due to overfitting, sensitivity to noise, and inability to effectively capture spatiotemporal dependencies in solar irradiance data. Moreover, most models are trained on horizontal irradiance measurements, which makes them less applicable for tilted surfaces where irradiance distribution is strongly influenced by tilt angle, azimuth, and diffuse radiation. Transposition models like the Horizontal Diffuse K Clearness Index Regression (HDKR) are widely used for tilted-surface estimation; however, their reliability depends on site-specific calibration and simplified assumptions about atmospheric conditions, which limit generalizability across different climates and geographies.

On the energy management side, rule-based EMS strategies are attractive for their simplicity and low computational requirements, yet they lack adaptability and fail to consider uncertainties from fluctuating irradiance and varying driving profiles, leading to suboptimal energy allocation between battery and ultracapacitor. Optimization-based methods such as Mixed-Integer Linear Optimization (MILO) provide more precise control but are computationally demanding and impractical for real-time driving scenarios. Similarly, predictive EMS approaches rely heavily on accurate forecasts and often break down when faced with forecast errors or unmodeled dynamic conditions. Collectively, these limitations reveal that existing methods are either too simplistic to handle variability or too complex to operate in real time, underscoring the need for a hybrid framework that combines the predictive accuracy of advanced machine learning models like LSTM with the practicality of enhanced rule-based EMS adapted for real-time HEV operation.

1.5. Contributions and Benefits

This paper addresses the aforementioned needs and challenges through the following contributions. First, it develops a deep neural network-based solar irradiance prediction model trained on site-specific data from Durg, Chhattisgarh (21.191°N, 81.299°E, 289 m elevation), ensuring high accuracy and contextual relevance. Second, it integrates the data into the HDKR model for tilted-surface irradiance estimation, directly applicable to HEVs with embedded PV modules. Third, it proposes a novel constraint-driven EMS that optimally coordinates battery and ultracapacitor storage, accounting for forecast uncertainty and seasonal variations. Fourth, it validates the proposed framework against real driving cycles, showing improvements in energy efficiency, reliability, and storage utilization compared with existing methods. The benefits of this research lie in enabling solar-assisted HEVs to meet power demand requirements more reliably, extend component lifetimes, and operate efficiently under variable driving and environmental conditions.

1.6. Paper Organization

The rest of the paper is organized as follows. The paper begins by addressing current transportation system issues and introducing the proposed model represented by Fig-1. Following that, it goes into elaborate detail describing the fundamental block diagram, component information, and ratings. Section 2 introduces the overall HEV architecture and describes system components. Section 3 presents the modified solar energy estimation model and HDKR integration. Section 4 explains the model implementation. Section 5 details the constraint-driven EMS and hybrid storage optimization. Section 6 reports simulation results and performance analysis. Finally, Section 7 concludes with contributions, limitations, and potential avenues for future research.

1.7. Proposed Framework

Fig. 1 show the proposed framework for Solar irradiance forecasting with modified interleaved and EMS technique.

2. SOLAR IRRADIANCE FORECASTING

2.1. Data Collection and Preprocessing

For the Durg, Chhattisgarh region, data is gathered via PVsyst Software and NASA's POWER Data Access Viewer. The global horizontal irradiance (GHI), temperature, dew point, wind speed, relative humidity, pressure, precipitable water, wind direction, and other meteorological characteristics are all included in the dataset. Furthermore, data on surface albedo, cloud type, ozone, solar zenith angle, and clear-sky irradiance are acquired. To guarantee data quality and consistency, preprocessing is done on the data before the machine learning models are trained. This includes resolving missing values, eliminating superfluous features (like fill flags), and generating numerical representations for categorical variables (like cloud type). To scale the features within similar categories and enhance the convergence and performance of the models, data normalization techniques are also employed. Neural networks are well-suited for solar prediction tasks that involve variables such as azimuth angle and zenith angle due to their ability to capture complex, non-linear relationships inherent in solar radiation dynamics.

Neural networks can handle historical sun radiation measurements and other related environmental variables because they can scale to analyse big datasets quickly. They are an effective tool for solar prediction applications owing to their capacity to adjust to shifting conditions and continue providing accurate forecasts over time. There are 21 properties in this dataset, of which 20 are input features that range from sun zenith angle to average barometric pressure. Our target variable, which expresses the amount of electricity produced by the PV module in kW, is represented by the remaining attribute [16].

2.2. Solar Prediction Using Neural Network

In order to produce expected outputs, input characteristics are fed via hidden layers throughout the forward propagation process. Activation functions, such sigmoid or RELU, play a crucial role in determining how each layer's output is shaped. The difference between predicted and actual outputs over several samples is measured by the mean squared error (MSE), which is often employed as the loss function to evaluate the neural network's performance. [17-19]. Readjusting network parameters, like weights and biases, depending on the calculated errors at each layer is made easier by the backpropagation method. Finally, weights and biases are iteratively updated using gradient descent optimization, which directs the network toward reducing the loss function. Neural networks provide a strong framework through this method for improving solar prediction accuracy, leading to more effective utilization of solar energy resources [20].

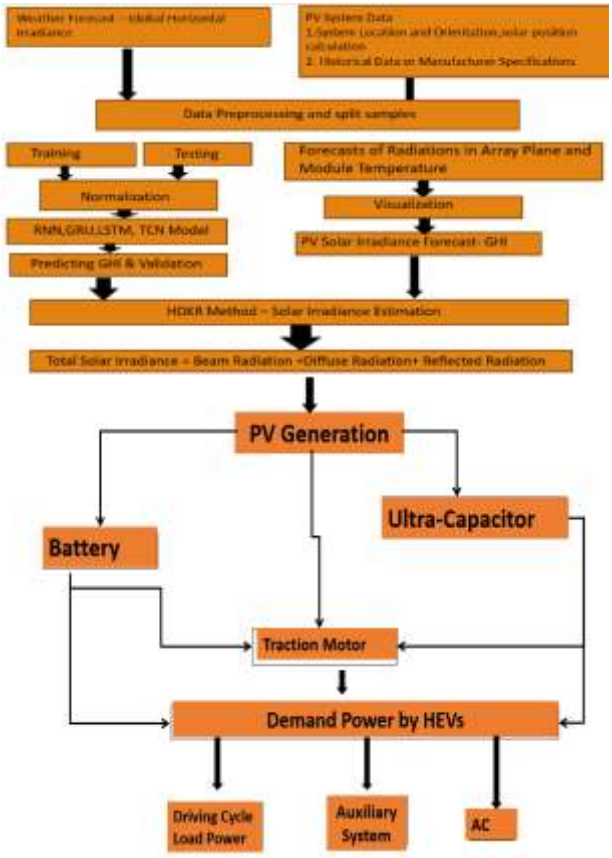


Fig. 1: Proposed block representation – Solar irradiance forecasting with modified interleaved and EMS technique.

3. MODIFIED SOLAR ESTIMATION FOR OPTIMAL ENERGY MANAGEMENT SYSTEM USING HDKR METHOD IN HEVS

Precise evaluation of solar radiation components, including beam and diffuse radiations, is required to optimize energy management strategies in electric vehicles. This paper proposes an improved methodology for an accurate calculation of solar radiation components on tilted surfaces using the Hay, Davies, Klucher, and Reindl (HDKR) technique. [21-22] The efficiency of the proposed methodology in improving the estimation of solar radiation's accuracy by thorough simulations experiments. Improved energy management and the incorporation of solar energy systems into electric vehicles configurations is implemented with this method. To calculate the diffuse and beam radiations on tilted surfaces more precisely, the HDKR technique incorporates a number of geometric and atmospheric factors. The HDKR method's primary steps are as follows:

3.1. Solar Time (t_solar)

Solar time (t_solar) is the time indicated by the position of the Sun in the sky. It accounts for variations in the Earth's rotation and orbit around the Sun. The formula to calculate solar time is given by (1) [38]:

$$t_{solar} = time + \frac{4.(logitude - logit_{zone}) + e}{60} \quad (1)$$

where:
- Time is the standard time.
- longitude is the observer's longitude.

- longit_zone is the standard time zone meridian.
- *e* is the equation of time.

3.2. Equation of Time (e)

The equation of time (e) represents the difference between mean solar time and apparent solar time. It is calculated using the following formula is given by (2):

$$e = 229.2* (0.000075 + 0.001869*\cos(b) - 0.032077 * \sin(b) - 0.014615 * \cos(2b) - 0.04089 *\sin(2b)) \quad (2)$$

where *b* represents the Earth's orbital position for a given day of the year.

3.3. Declination Angle (δ)

The declination angle (delta) indicates the angle between the rays of the Sun and the plane of the Earth's equator. It is calculated using the formula:

$$\delta = 23.45* \sin(360 *(284 + day)/365) \quad (3)$$

where day represents the day of the year.

3.4. Solar Azimuth Angle

The horizontal direction of the Sun with respect to a reference direction is indicated by the solar azimuth angle. The latitude, declination angle, and solar zenith angle of the observer will be utilized to calculate it. The equation is given by (4):

$$\text{Solar_azimuth} = \text{sign}.\cos^{-1}\left(\frac{\cos(solar_{zenith}).\sin(latitude)-\sin(\delta)}{\sin(solar_{zenith}).\cos(latitude)}\right) \quad (4)$$

whare Sign = 1 if $t_{solar} \geq 12$, otherwise Sign = -1

3.5. Incidence Angle (Θ)

The angle formed by the direction of incoming solar radiation and the normal vector to a surface is called the incidence angle (σ). It is computed by (5) as follows [39]:

$$\Theta = \cos(\text{solar_zenith}) * \cos(\text{tilt_angle}) + \sin(\text{solar_zenith}) * \sin(\text{tilt_angle}) \cos(\text{solar_azimuth} - \text{surface_azim}) \quad (5)$$

3.6. Solar Radiation (G_{sc}, $G_{horizontal_radiation}$)

Solar radiation refers to the electromagnetic energy emitted by the sun and received at a particular location on Earth's surface. The average solar irradiation at the top of the earth's atmosphere is represented by the solar constant (Gsc). The radiation formula is given by (6) in the horizontal direction.
Solar Radiation ($G_{horizontal_radiation}$)

$$G_{horizontal_radiation} = Gsc *(1.000110 +034221 *\cos(b) +0.00128\text{sib(b)} + 0.000719*\cos(2b) +0.000077*\sin(2b)) \quad (6)$$

3.7. Clearness Index (K_t) and Diffuse Fraction (R_{od})

The clearness index (K_t) represents the ratio of the solar radiation measured on a horizontal surface to the extraterrestrial solar radiation. The diffuse fraction (R_{od}) indicates the fraction of total solar radiation that is diffuse rather than direct radiation. (K_t)and (R_{od}) are calculated using the provided formulasby (7)[40].

$$K_t = \frac{G_{horizontal_radiation}}{\text{solar}_{\text{radiation}} * \cos(\text{solar}_{\text{zenith}})}$$

$$R_{od} = \begin{cases} 1 - 0.249 * K_t \text{ , if } K_t \leq 0.35 \\ 0.177, if\ K_t > 0.75 \\ 1.557 - 1.84 * K_t, otherwise \end{cases} \quad (7)$$

The ratio of solar radiation measured on a horizontal surface to solar radiation from extraterrestrial sources is known as the clearness index (K_t). The percentage of total solar radiation that is diffuse rather than direct is known as the diffuse fraction, or R_{od}. The given formulas are used to determine (K_t) and (R_{od}) by (8)[41].

$$K_t = \frac{GHI}{clear-skyGHI} \quad (8)$$

The key steps involved in the HDKR method include:

1. *Beam radiation calculation:* To determine the incidence angle modifier (δ) and use it to modify beam radiation in order to obtain beam radiation on tilted surfaces (G_{beam}).

2. *Diffuse Radiation Calculation:* The isotropic sky diffuse radiation (G_d), which is an approximation of the diffuse radiation originating from the sky dome as a whole, is determined. Making use of the tilt angle to modify the isotropic sky diffuse radiation in order to obtain the diffuse radiation on the tilted surface. Compute the circumsolar diffuse radiation as well, which is the diffuse radiation originating from a given angular radius surrounds the solar disk.

3. *Beam and Diffuse Radiations:* Add the beam and diffuse radiations to get an estimate of the total radiation on the slanted surface by (9).

Total solar Radiation = Beam Radiation + diffuse radiation + reflected radiation. (9)

4. Model Implementation

The model is applied and the accuracy of the GHI projections for 2024 is determined using meteorological data ranging 2019 to 2024. While the input features include GHI, meteorological information, and the clearness index for the previous 24 hours, the output includes the total GHI for the next hour and the next 24 hours. The model design uses a single hidden layer structure with a sigmoidal activation function to handle gradient dispersion and computation performance. On the hidden layer, dropout regularization is applied to minimize overfitting. The output layer computes the loss function between the target and predicted outputs, giving the Mean Absolute Error (MAE). The obtained gradients are used by the backpropagation (BP) technique to adjust the network weights.[17] The Adam algorithm is used to create optimization parameters till convergence. The model applies denormalization to the output after training to pair the predicted values with the corresponding time-series data.

4.1. Performance Evaluation Metrics

Four error metrics were evaluated for evaluating the forecasting model's performance using equations (10) and (11):

1. Root Mean Square Error (RMSE): This measures the difference between predicted and actual values. Better predicting accuracy is shown by a lower RMSE. The equation is:

$$\textbf{RMSE} = \sqrt{\frac{1}{N}\sum_{i=1}^{N}((P_f - P_a)^2} \quad (10)$$

where N is the number of observations, P_f is the forecast value, and P_a is the actual value.

2. R-Squared (R^2): R-Squared, which goes from 0 to 1, evaluates how well the predictive model fits the data. Better fit is indicated by a higher value. The formula is given by the following equation [18]:

$$R^2 = 1 - \frac{\sum_{i=1}^{N}((P_f - P_a)^2}{\sum_{i=1}^{N}((P_f - P_a)^2} \quad (11)$$

The computational model is developed using the Julia programming language (version 1.4.0) in conjunction with the JuMP optimization package (version 0.21.2), both of which are open-source and publicly accessible. For solving the formulated optimization problem, the Gurobi solver (version 0.76) is employed under an academic license.

5. SCHEDULED CONSTRAINED DRIVEN ENERGY MANAGEMENT STRATEGY

The objective of the paper is to meet specific electrical energy requirements for both the driving cycle and auxiliary systems by optimizing the operation of an integrated energy management system. By the investigation of a model vehicle equipped with a photovoltaic system, battery, and ultracapacitor for energy storage, the research evaluates whether different configurations and objectives impact significant metrics for performance [23]. The study analyses optimal energy flows with hourly resolution over a year, taking into account complicated dependencies and technical constraints, using Mixed-Integer Linear Optimization (MILO). Attention is placed on the different modes of power consumption of the modulating traction motor during the driving cycle and while the auxiliary system is operating. To guarantee reproducibility and transparency, the study provides models, parameters, and visualization code. This study analyses the flow variable given in Table 3. the operational control of a traction motor and PV system [24]. They differentiate between predictive and nonpredictive approaches, with nonpredictive methods relying on rule-based or schedule-based algorithms [25-27]. In these approaches, the traction motor is activated based on

Table 1: Pseudo-code for ANN-based solar forecasting algorithm.

Preprocess data:
-Number of Samples:15000,60% for Training and 40% for Test;
-num_epochs = 100, batch_size = 32, num_hidden_neurons = 256, num_input_neurons = 87

Adding azimuth angle and incidence angle to input neurons
num_output_neurons = 1

Train the model
-for epoch in range(num_epochs):
-for batch_idx in range(len(X_train_batches)):

Get the current batch
- X_batch = X_train_batches[batch_idx]
-y_batch = y_train_batches[batch_idx]

Forward propagation
Extract azimuth angle and incidence angle from X_batch
-azimuth_angle = X_batch[:, -2] # Assuming azimuth angle is the second last column
-incidence_angle = X_batch[:, -1] # Assuming incidence angle is the last column

Concatenate azimuth angle and incidence angle with input features
-X_batch_with_angles = np.concatenate((X_batch[:, :-2], azimuth_angle[:,np.newaxis], incidence_angle[:,np.newaxis]), axis=1)

Compute hidden layer activations
-a_hidden = np.dot (X_batch_with_angles, W_hidden) + b_hidden

Apply activation function
-a_hidden = np.maximum (a_hidden, 0)

Compute output layer activations
- y_pred = np.dot (a_hidden, W_output) + b_output

Compute loss (e.g., mean squared error)
- loss = np.mean((y_pred - y_batch) ** 2)

Backpropagation & Compute gradients
-delta_output = y_pred - y_batch
-delta_hidden = np.dot (delta_output, W_output.T) * (a_hidden> 0)

Update weights and biases
-W_output -= alpha * np.dot (a_hidden.T, delta_output)
- b_output -= alpha * np.mean(delta_output, axis=0)
-W_hidden -= alpha * np.dot (X_batch_with_angles.T, delta_hidden)
-b_hidden -= alpha * np.mean(delta_hidden, axis=0)

Optionally, print loss or other metrics
-if batch_idx % 10 == 0:
-print (f'Epoch {epoch+1}, Batch {batch_idx+1}, Loss: {loss:.4f}')

Evaluate the model on the testing set
-y_pred_test = np.dot (np.maximum(np.dot(X_test, W_hidden) + b_hidden, 0), W_output) + b_output

Compare the real data with the predicted data

Table 2: Ratings of the hybrid electric vehicle.

Parameter	Value	Parameter	Value
Battery Type	Li-ion	Cells in Module	3 in series
Battery Cell	40 Ah/60V	Battery Modules	31 in series
Battery Cell	0.378 kg	Maximum Capacity (Ah)	40
UC Type	PC2500	UC Cells	120
UC Voltage	225V	UC Capacitance	58F
UC Resistance	0.02	Battery Efficiency	88
HEV MASS	830kg	PV Cell Voltage	27.3
Frontal Area	2.03 m^2	PV Cells in series and parallel	20 & 3
Motor Type	IM (AC75)	Motor Torque scale	0.268
Motor Power	20kW	Initial Temp.	30 °C
Cargo	136kg	Average Load	1.28
Input Neurons	6	Hidden Layer	2 layers
Neurons per hidden layer	20	Activation Function	ReLU (Hidden Layers), Linear (Output Layer)
Batch Size	32	Learning Rate	0.001
Training Epochs	300	Regularization	Dropout (0.3), L2 (0.0005)
Optimizer	Adam	Weight Initialization	Xavier

Table 3: Flow variables.

Demand Fulfillment	C_{pv}-E_{demand}, C_{bat}-E_{demand}, C_{UC}-E_{demand}, C_{pv}-$_b$. C_{pv}-$_{UC}$
Traction Motor inflows	C_{pv}-$_{Tr}$, C_{UC}-$_{Tr}$. C_b-$_{Tr}$
Traction Motor modulation	C_{Tr}-$_{Driving\ cycle}$, C_{Tr}-$_{AC}$

predefined condition on time etc. The hybrid energy management system (HEMS), consists of a traction motor (Tr), ultracapacitor (UC), battery (B), and PV system (PV). The vehicle's auxiliary system and driving cycle can both be powered by the traction motor. The study includes the following known parameters: the external temperature ($T_{external}$), PV generation (C_{pv}), driving cycle demand (C_{dc}), auxiliary system demand (C_{Paux}), and electricity demand (E_{demand}).By the setting of a one-year control horizon at a time resolution of one hour, for the fundamental features of the most effective control strategy. The PV system ($C_{Ppv}\rightarrow E_{demand}$), battery ($C_{bat}\rightarrow E_{demand}$), or ultracapacitor ($C_{UC}\rightarrow E_{demand}$) can supply the power flow required to satisfy electricity demand (E_{demand}).

It guarantees that the entire amount of power generated is equal to the sum of the flows from the PV system to meet demand, storage devices, ultracapacitors and traction motors. The energy balance of the battery state of charge (SOC_b) is computed using (13). SOC_b rises when the PV system's electricity supply rises ($C_{Ppv}\rightarrow C_b$), and it falls when the traction motor ($C_{bat}\rightarrow C_{TR}$) or the battery supplies electricity to meet demand ($C_{bat}\rightarrow E_{demand}$).
Three sources can supply electricity to the traction motor: the ultracapacitor ($C_{PUC}\rightarrow C_{Tr}$), the PV system ($C_{Ppv}\rightarrow C_{Tr}$), or the battery ($C_{Pb}\rightarrow C_{Tr}$). It functions in two modes: $C_{PTR}\rightarrow C_{DC}$ for the driving cycle and $C_{TR}\rightarrow C_{AUX}$ for the auxiliary system, which reflect different energy flows. The driving cycle (C_{ModDC}) and auxiliary modes (C_{ModAUX}) modulation degrees are continuous variables with a range of zero to one.

Objective Function: $J = \sum_{t=1}^{N}(PV_t + AC_t + DC_t$ (12)

Subject to the following constraints:
Energy balance constraint:

$$AC_t + DC_t + SOC_t - SOC_{t-1} = PV_t - C_{loss} \cdot \left| SOCt - SOC_{t-1} \right|$$

State of charge constraints: (13)

$SOC_{min} < SOC_t < SOC_{ma}$

Non-negativity constraints:

$AC_t \geq 0, DC_t \geq 0, SOC_t \geq 0$

where $C_{PV\text{-}DC}(t)$, $C_{b\text{-}DC}(t)$, $C_{UC\text{-}DC}(t)$ represents the energy flow from PV system to battery, ultracapacitor and the grid to the driving cycle and AC at time t respectively. $C_{PV\text{-}DC}(t)$, $C_{PV\text{-}AC}(t)$, $C_{PV\text{-}B}(t)$, $C_{pv\text{-}UC}(t)$, the energy flow from the PV system to the driving cycle, AC, battery, PV, grid at time *t* respectively. The objective function J given by equation in 12 continues to represent the overall energy consumption across the time horizon *N* in this extended formulation. All time intervals' energy consumption terms for the PV, AC, and DC cooling systems are added together. Every time step, energy generation, consumption, and storage are balanced due to the energy balance constraint. The term that penalizes differences in the state-of-charge between consecutive time intervals is used to account for energy losses $C_{loss.}\left| SOCt - SOC_{t-1} \right|$.In order to guarantee that the energy storage system functions within its capacity limitations, the state-of-charge constraints limit the SOC within permissible parameters are SOC_{min} to SOC_{max}. Energy consumption and state-of-charge must both remain non-negative during the optimization phase due to the non-negativity restrictions AC_t and DC_t given by (13).

Flow constraints:

$C_{PV\text{-}DC(t)} + C_{B\text{-}DC}(t) + C_{UC\text{-}DC}(t) = DC(t)$ (14)

$C_{PV\text{-}DC}(t)+ C_{PV\text{-}B}(t)+C_{pv\text{-}UC}(t)+C_{PV}\text{-}AC(t) = GE(t)$

Battery constraints:

$$SOC_b(t+1) = (1\text{-}loss_b) *SOC_b(t) + \eta_b *C_{PV\text{-}B}(t) - \left(\frac{Cb-DC(t)+Cb-Tr(t)}{\eta b}\right)$$
$$SOC^b_{min} \le SOC_b(t) \le SOC^b_{max} \quad (15)$$
$$C_{B-DC}(t), C_{PV-B}(t), C_{B-DC}(t) \le B_{\max,\text{rate}}$$

where, $SOC_b(t)$ denotes the state of charge of battery at time t, $Loss_b$ represents the energy loss factor of the battery, η_b is the efficiency of the battery, SOC^b_{min} and SOC^b_{nmax} denotes the maximum and minimum allowable state of charge for the battery, $B_{\max,\text{rate}}$represents the maximum charging/discharging rate of the battery.

The constraints given by (14) and (15) ensure that energy flows and state of charge levels of the battery, ultracapacitor and PV for increasing the efficiency of electric vehicle. Let P_{demand} be the power demand, P_{min} be the minimum power, P_{PV} be the power of PV, P_{bat} be the battery power and P_{UC} be the UC Power. The system power supply hierarchy can be represented by (16) and (17):

P_{supply} =

P_{PV} , if $P_{PV} \ge P_{min}$

P_{bat} , if $P_{PV} < P_{min}$ and $P_{bat} \ge P_{min} - P_{PV}$ (16)

P_{UC} , if ($P_{PV} < P_{min}$) and ($P_{bat} < P_{min} - P_{PV}$) and ($P_{UC} \ge P_{min} - P_{PV} - P_b$)

P_{ICE} , otherwise

Under regenerative mode:

$P_{UC,Charge}$ =

0 , if $P_{demand} \ge 0$

$\alpha \cdot P_{PV,excess_}$, if ($P_{demand} < 0$) and ($P_{UC_SOC} < P_{UC_MAX_SOC}$) (17)

$\beta \cdot (P_{demand} - P_{PV,excess})$, if ($P_{demand} < 0$) and ($P_{UC_SOC} \ge P_{UC_MAX_SOC}$)

where $P_{PV,excess} = \max(0, P_{PV} - P_{PVmax})$

Traction motor constraints:

$C_{TR}(t) = C_{PV\text{-}TR}(t) + C_{B\text{-}TR}(t)$

$C_{TR}(t) \le T_{Rmax_power}$

$C_{TR\text{-}DC}(t) + C_{TR\text{-}AC}(t) = C_{PV\text{-}TR}(t) _ C_{UC\text{-}TR}(t) + C_{B\text{-}TR}(t)$

$C_{TR\text{-}DC}(t) = Mode_{DC}(t) * DC_{max_power}$ (18)

$C_{TR\text{-}AC}(t) = Mode_{AC}(t) * DC_{max_power}$

$Mode_{DC}(t) * T_{Rswitch}(t) \le DC_{max_power}$

$Mode_{AC}(t) * (1 - T_{Rswitch}(t)) \le 1 - T_{R\ max_power}$

Air Conditioning (AC) constraints

$$C_{AC}(t) = Cpv\text{-}tr(t) + C_{B\text{-}AC}(t) + C_{UC\text{-}AC}(t)$$
$$C_{AC}(t) \le AC_{max_power} \quad (19)$$

where $C_{TR}(t)$ and $C_{AC}(t)$ represents the power consumed by the traction motor and air conditioning unit at time t.$C_{PV\text{-}DC}(t)$, $C_{PV\text{-}B}(t)$, $C_{PV\text{-}UC}(t)$ and $C_{PV\text{-}TR}(t)$ represents the flows of energy from PV system to driving cycle cooling system, battery, ultracapacitor and traction motor at time t respectively. $SOC_B(t)$ and $SOC_{UC}(t)$ are the state of charge of the battery, ultracapacitor at time interval at time t. $Loss_b$ represents the energy loss factor of the battery.η_b is the efficiency of the battery. SOC^b_{min} and SOC^b_{max} denotes the minimum and maximum allowable state of charge for the battery, respectively.$B_{\max,\text{rate}}$ represents the m, maximum charging/discharging rate of the battery represented by (18) and (19).

6. Simulation Results- Comparing Predicted vs. Measured Performance of Photovoltaic Modules

For solar power plants to operate and be controlled effectively, solar power forecasting is essential. The amount of energy generated by the solar photovoltaic (PV) array is affected by various external environmental factors, including dust deposition on the panels, humidity, air temperature, and solar radiation. These factors also include the doping level and design of the PV array. These naturally fluctuating components have a direct effect on the manufacturing of solar cells. In addition, variations in solar irradiation and the previously mentioned environmental conditions take place during the day. To enhance the accuracy of PV module output forecast and, consequently, the efficiency of solar power plants, it is essential to measure and evaluate the hourly averages or specific intervals of these parameters.

The dataset includes several metrics that are essential for projecting solar electricity and operating plants, including:

1.Power generated: The joules of energy produced in three hours.

2. Distance-to-solar-noon: This is a radian-based measurement of the angular separation from solar noon.

3. Temperature: In degrees Celsius, the average daily temperature.

4. Wind direction: The degree of average daily wind direction, from 0 to 360.

5. Wind speed: An average daily wind speed expressed in meters per second.

6. Sky cover: Displayed as a five-step scale, where 0 represents complete visibility and 4 represents complete coverage.

7. Visibility: Kilometres are used to express visibility.

8. Humidity: expressed as a percentage.

9. Average wind speed (period): The average wind speed over the three hours of data, expressed in meters per second.

10. Mean pressure (time interval): Mean barometric pressure during the 3-hour period when measurements were taken, in inches of mercury.

The complex dynamics of Root Mean Squared Error (RMSE) during the training of an artificial neural network (ANN) are depicted in Fig. 2. Over multiple epochs, the paper thoroughly monitors variations in RMSE. By analysing these patterns, the article offers profound insights into the convergence dynamics of the ANN and its capacity to generalize to unknown input. The graphic illustrates how the RMSE drops to 0.2694 as the number of epochs increases, highlighting how effective the training process is at lowering error and improving model performance [23].
With the help of the provided code, a visualization is created to compare a model's prediction accuracy to the actual values for the training and test datasets shown in Fig. 3. The subplot on the left, where real generated power is displayed on the y-axis and expected power output is plotted on the x-axis, displays the evaluation of prediction accuracy for training data. Similarly, the accuracy of test data prediction is evaluated in the subplot to the right. The comparison between the predicted and actual power output values in the image provides insight into how well the model caught the underlying patterns in the data.

The model provided generates a graphic to compare predicted generated power levels with actual values based on the sun azimuth angle in Fig. 4. The left subplot displays the evaluation of training predictions against the solar azimuth angle. Real generated power levels and anticipated power outputs are displayed using scatter graphs. The sun azimuth angle is represented by the x-axis, while the training data is shown by the y-axis. Similarly, the right subplot shows the assessment of test predictions concerning the sun azimuth angle. Both subplots show how the model can predict power production based on variations in the sun azimuth angle.

Following the training and testing phases, the model's performance was thoroughly examined using random datasets to cover a range of epochs, from 2 to 16. The method conducted a thorough comparison between the real and projected datasets in order to provide light on how epoch changes affect prediction accuracy. A thorough analysis of the variations between the actual and predicted values throughout several epochs yielded important insights into the model's ability to adapt and generalize to a range of datasets. The comprehensive research demonstrates the artificial neural network model's stability and offers guidance on the optimal epoch selection to maximize prediction performance in Fig. 5.

6.1. Performance comparison of Forecasting techniques

Metrics like mean square error (MSE) and root mean square error (RMSE) are used to assess the quality of predictions. Model optimization and fine-tuning depend significantly on the accuracy and validity information these

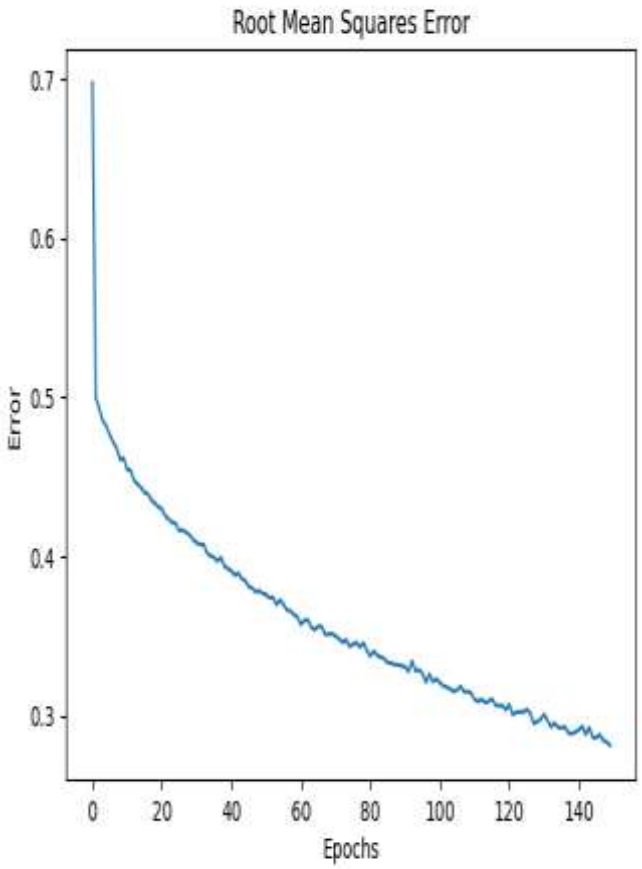


Fig. 2: Root mean square error evolution across epochs.

measures deliver. There are notable correlations between a number of solar and meteorological-related parameters.

1. The angle of incidence and zenith have a strong positive association (0.71)

2. The relationship between generated power in KW and backward shortwave radiation is 0.56.

3.Relative humidity and low cloud cover (0.49) and zenith (0.51) are positively correlated.

4. The Angle of Incidence and Zenith and Generated Power have a substantial negative association (-0.65).

5. Temperature and zenith have an inverse relationship (-0.55).

6. There is a high negative correlation (-0.8) between shortwave radiation backward and Zenith.

7. The relationship between shortwave radiation and relative humidity (-0.72) and the relationship between temperature and relative humidity (-0.77) are negative shown in Fig. 5.

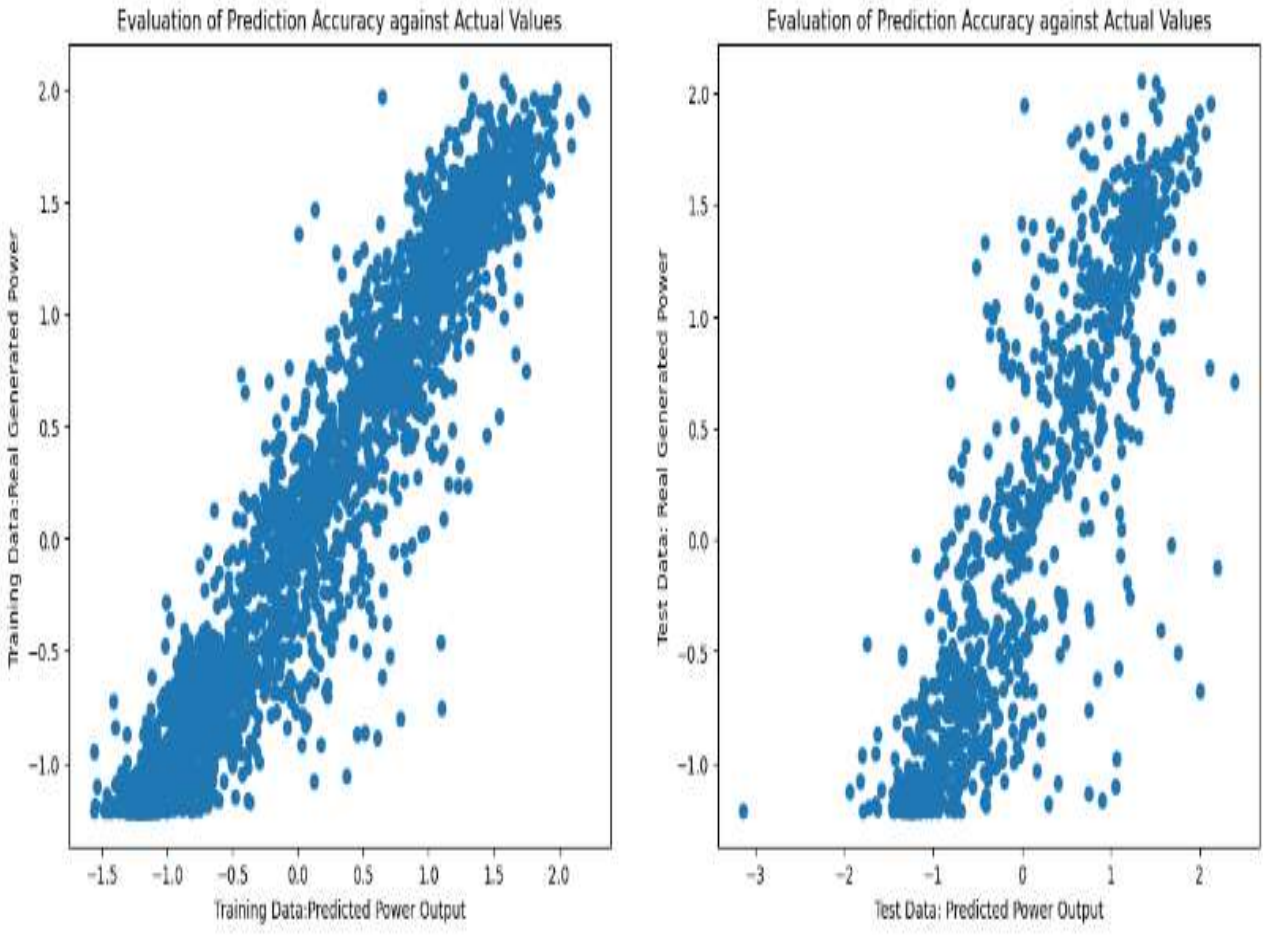


Fig. 3: Epoch-based evaluation of solar power prediction accuracy: Insights from training and test data.

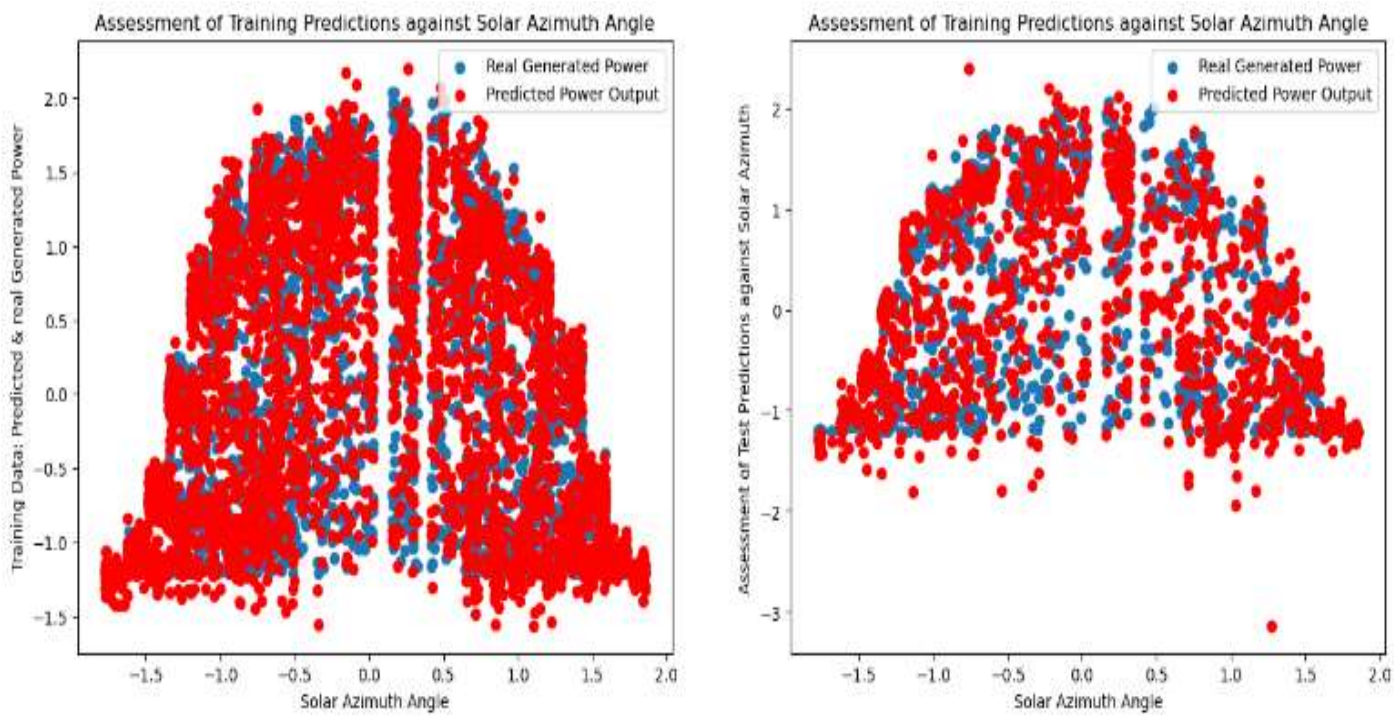


Fig. 4: Visualization of solar power prediction accuracy based on solar azimuth angle.

By comparison, given in Table 4, the proposed LSTM–HDKR-based method in Chhattisgarh, India (latitude 21.2085°N, longitude 81.3482°E), achieved $R^2 = 0.8818$ and RMSE = 0.269**,** which indicates strong predictive capability

	Real Solar Generated Power	Predicted Solar Power Output
2	-0.82	-1.41
3	-0.87	-0.89
4	1.33	1.41
5	1.17	1.14
6	0.74	1.04
7	1.13	1.68
8	0.12	-0.29
9	1.60	1.78
10	0.95	0.25
11	1.24	0.67
12	1.63	1.97
13	1.79	1.34
14	-0.90	-1.23
15	2.06	1.35
16	1.42	-0.01

Fig. 5: Solar Irradiance on random testing data sets.

with very low error despite high variability in local climatic conditions. This comparison highlights that while some existing methods show higher correlation coefficients, the proposed approach delivers superior robustness by minimizing prediction errors, making it more suitable for integration into hybrid electric vehicle energy management systems.

6.2. Functionality Test

During the functional test, the PV-UC-battery HEV is simulated to operate in multiple modes during a driving cycle, such as idling, starting, cruising, accelerating, and regenerative braking [22]. The simulation results, which are shown in Table 5 with the initial battery state of charge (SOC) at 75% and varying solar radiance and ambient temperature, demonstrate how various power sources connect. The battery serves as the main power source. High solar radiation and a high state of charge (SOC) of the battery indicate solar energy charging, which is indicated by negative battery power during vehicle pauses. The vehicle is propelled forward by its photovoltaic array and batteries until increased power requirements compel the ultracapacitor (UC) to come on. The battery absorbs excess UC power. when the demand for power decreases, the excess UC power is stored in the battery. The battery becomes the primary power source once the motor reaches its maximum output.

Data from the Mahindra Hybrid Electric Vehicle Research Centre was acquired, with a specific focus on a small vehicle model, in order to establish the monthly usage of power. The driving cycle and the Air Conditioning (AC) system are the two primary aspects of the analysis. First, the amount of electricity used for driving was determined, paying close attention to factors including road conditions, vehicle speed, acceleration, and deceleration patterns. This comprehensive assessment provided valuable insights into the energy demands of the vehicle's propulsion system across various driving scenarios. In addition, the amount of electricity used by the air conditioning system was assessed, taking into account variables such as user preferences, cabin size, and outdoor temperature. Through the analysis of these variables, a comprehension of the monthly electricity usage for both the driving cycle and the AC system came to pass. The model is optimized using the Gurobi solver (package version 0.7.6) with an academic license.

The study makes it easier to estimate accurately and create energy-management plans that work for the unique features of Mahindra's compact car type. The graph in Fig. 6 illustrates the amount of electricity used each month for driving cycles, demonstrating how the amount of energy consumed varies over time. Energy efficiency techniques can be optimized by gaining insights into seasonal fluctuations and driving patterns through the analysis of these trends. This graphic depiction is an excellent tool for comprehending the dynamics of vehicle energy consumption and providing guidance for energy management decisions. The graphic in Fig. 7 also shows the vehicle's AC system and auxiliary devices of the vehicle's monthly electricity use, highlighting usage trends and seasonal fluctuations. The significant bars seen in green on the graph suggest higher AC demand in the summer, especially in April, May, June, and July. Blue represents other auxiliary devices, including lighting and music.

Table 4: Performance comparisons.

References	Location	Latitude/Longitude	Findings
RahimiKhoob[32]	Spain	36.834N/2.463W	R2 =0.889 RMSE= 2.53
A.M. Pavan[33]	India	9.9252N/78.1198E	R2 =0.99 RMSE= 4.832
A. Assi[34]	UAE	24.1302N/55.8023E	R2 =0.93 RMSE= 0.43
C. Muraleedharan[35]	India	23.2599N/77.4126E	R2 =0.9989 RMSE= 0.5016
Proposed Method	India Chhattisgarh	21.2085N, 81.3482E	R2=0.8818 RMSE=0.269

Table 5: Annual key performance indicators for different driving conditions and AC status.

Case	AC Status	Driving Conditions (UDDS)	AC Temperature (°C)	Energy Consumption (kWh)	Battery Satisfies Demand(%)	UC satisfies Demand(%)	PV satisfies Demand(%)	Run Time	Mean SOC Battery wrt to target SOC
Case-1	On	Normal	20	8789	70	20	90	47	94%
Case-2	Off	Normal	-	8902	30	10	80	39	60.06%
Case-3	Off	Extreme Hilly,Terrain	-	8515	80	40	60	14	62.57%
Case-4	On	Extreme	24	8639	60	30	70	17	56.47%

6.3. Driving Cycle Scenarios

The standard condition for evaluating the performance of the lightweight battery-PV-UC HEV (Hybrid Electric Vehicle) system under the defined driving cycle conditions. To represent different battery statuses and environmental situations, three distinct scenarios are created:

Scenario 1: Sunny solar radiation - The PV array charges the battery to 75% capacity when it first starts.

Scenario 2: Overcast/rainy - In low solar radiation conditions, the PV output is insufficient, with the battery at 35% of its full charge.

Scenario 3: At night, solar radiation: 0 W/m2 - The vehicle is solely powered by the UC and battery, which results in a 55% state of charge for the battery.

Fig. 6 illustrates the energy distribution in the PV-UC-Battery HEV power system as well as the battery level of charge under Scenario 1. Because of the high output power generated by the PV array in Fig.9, the PV and the battery is used primarily as the power source under EMS control. The UC idles and operates in a low power range when its system efficiency is relatively high during periods of low power demand. Fig.9 demonstrates how the battery discharges to gradually decrease its state of charge as its energy storage is used as efficiently as possible to maximize solar energy utilization.

Figs. 6 and 7 analyse into the most effective methods for utilizing ultracapacitors, battery storage, and PV charging to meet the power needs of traction motors, air conditioning (AC), and driving cycles in an electric vehicle system. Seasonal analysis shows patterns of dynamic energy generation and consumption, with PV charging being essential to balancing power needs. Edge cases highlight situations in which energy production might not meet demand, requiring effective use of battery and ultracapacitor storage to close the gap and meet power requirements. The operational patterns observed in these situations provide insight into the extent to which energy management techniques work to balance the supply and demand of energy under varied driving circumstances and environmental variables. Furthermore, investigates the way driving cycles and AC usage affect energy consumption and storage dynamics, emphasizing the significance it is to optimize energy flows for improved vehicle economy and performance.

This subsection explores optimal flows with a battery and UC feed in addition to our initial objective function, which was power demand fulfilment. Fig.7 provides a description of seasonal fluctuations by displaying the seasonal mean PV generation (yellow line), matching sinks (stacked bars), and the mean battery State of Charge (SOC) (black line). Notably, as shown by the grey bars in Fig.7, there is a natural increase in UC during the summer, which is marked by low heating demand and high PV generation. In contrast to other seasons, the summertime battery SOC is lower, which highlights the influence of seasonal fluctuations on system behaviour. Notably, as shown by the grey bars in Fig. 7, there is a natural increase in UC during the summer, which is marked by high cooling demand and high PV generation. In contrast to other seasons, the summertime battery SOC is lower, which highlights the influence of seasonal fluctuations on system behaviour. One notable observation is that, as the day rolls on, self-discharging losses tend to cause battery charging to be delayed. However, certain anomalies to this pattern highlight how important it is to consider the time of day and seasonality when choosing the best charging tactics. Fig. 7 does not make it easier to analyse daily operating patterns, even though it provides insights into aggregated seasonal flows. The next paragraphs explore operational trends that are seen in the winter and summer, with a particular emphasis on specific edge cases. Winter presents unique challenges due to its combination of high heating demand and low PV generation.

The seasonal variations and anomalies observed in Fig. 7 further highlight the limitations of conventional static SOC strategies, which rely on fixed upper and lower SOC thresholds and fail to adapt to real-time fluctuations in load demand and solar irradiance. Traditional static methods often result in delayed charging, inefficient power distribution, and excessive battery stress during seasonal extremes. In contrast, the dynamic SOC control proposed in this research continuously adjusts the SOC reference in response to predicted solar irradiance (via the LSTM–HDKR model), instantaneous driving cycle conditions, and seasonal variability. This enables adaptive power sharing between the battery and ultracapacitor, ensures efficient utilization of available PV power, and prolongs battery life by avoiding repetitive deep discharges. Therefore, the proposed method provides a more resilient and adaptive energy management approach compared to static SOC targets, particularly under conditions of fluctuating renewable generation and variable driving patterns.

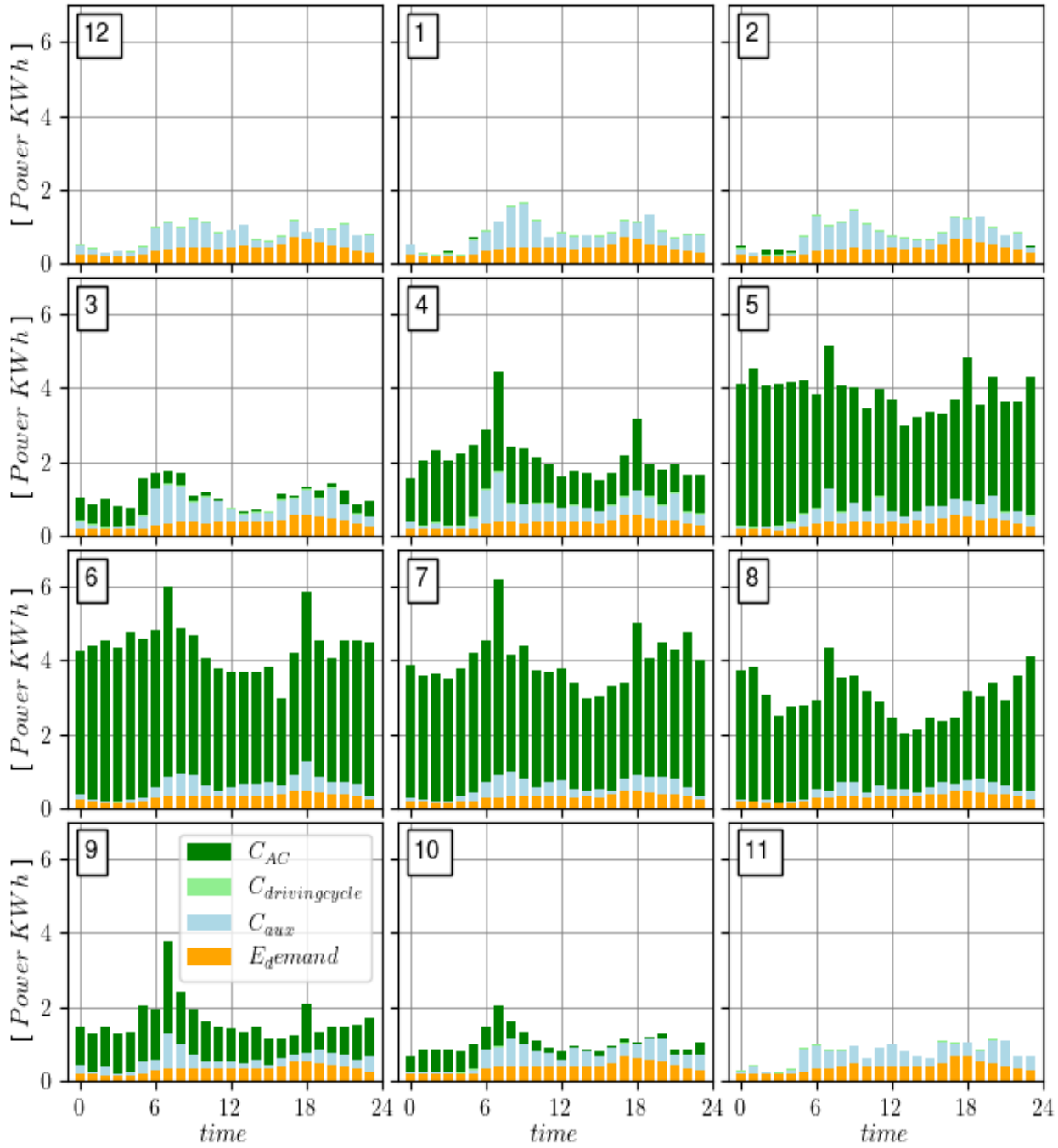


Fig. 6: Seasonal energy allocation for driving, AC, and Auxiliary systems by EMS battery, UC, and PV.

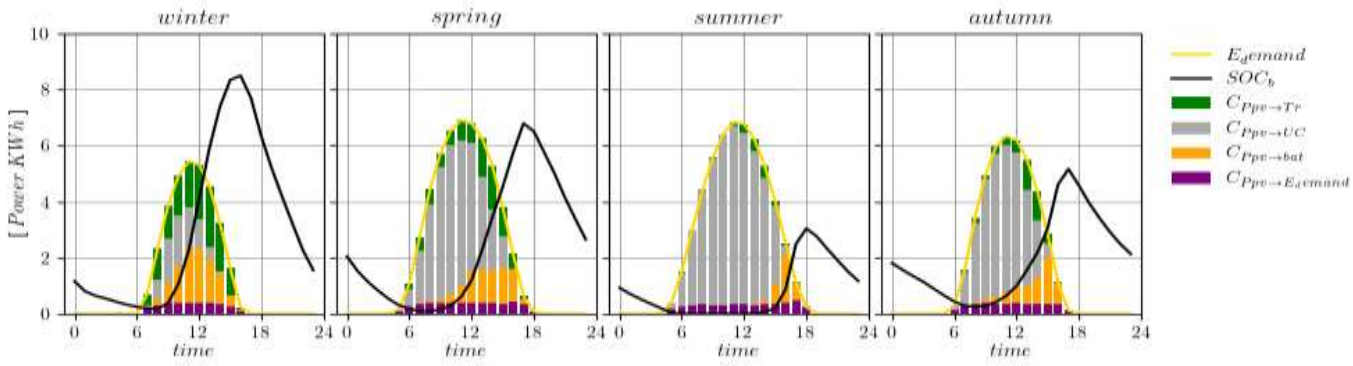


Fig.7: Seasonal distribution of average PV system flows and battery state of charge.

6.4. Optimizing Battery Performance with Dynamic Target State of Charge Control

Research suggests the median battery values exhibit behavior associated with battery characteristics, as they approach capacity limitations during winter and decrease to approximately 25% of the capacity in summer. To reduce dissipation losses, charging strategies were designed to match PV power surplus to the grid and to line with the current demand. Modelling limitations, such as restricted battery charge capacity because of PV generation or inverter capacity, were the cause of the lower SOC data. On the other hand, observations that were higher than the median, especially during seasonal variations, indicated a range of summertime AC cooling needs. It was suggested that target SOC levels be dynamically controlled, with adjustments made for daily, monthly, or seasonal mean SOCs. This could potentially increase net profits and decrease dissipation losses while maintaining user comfort.

Research suggests the median battery values exhibit behaviour associated with battery characteristics, as they approach capacity limitations during summer and increase to approximately 25% of the less capacity in winter. In order to reduce dissipation losses, charging strategies were designed to match PV power surplus to the grid and to line with the current demand. Modelling limitations, such as restricted battery charge capacity because of PV generation or inverter capacity, were the cause of the lower SOC data. On the other hand, observations that were higher than the median, especially during seasonal variations, indicated a range of summertime AC cooling needs. It was suggested that target SOC levels be dynamically controlled, with adjustments made for daily, monthly, or seasonal mean SOCs as shown in Fig.9. This could potentially increase net profits and decrease dissipation losses while maintaining user comfort. Future implementations must strike a balance between information needs and potential cost savings, which has interesting implications for rule-based control approach design. A prioritization framework is developed for distributing available PV generation within the integrated vehicle system, specifically for powering the air conditioning (AC) system and meeting cooling demands during driving cycles, through a thorough analysis of optimal energy allocation. At first, the priority was meeting the demand for electricity needed for cooling and vehicle running.

Subsequently, the focus was on preserving storage unit target state-of-charges (SOCs) in order to guarantee the best possible use of energy resources. The extra PV energy was then used to run the air conditioning system or stored for later use. We maximized energy use, especially during moments of high cooling demand, by calculating target SOCs and creating charging plans. Unlike traditional methods, this methodology enables dynamic SOC control according to driving conditions and climatic variables. This method allows for dynamic SOC management depending on driving circumstances and climate variations, which goes beyond traditional fixed rule-based approaches and requires additional testing using a variety of operational datasets from simulation studies. The energy flow depicted in Table 5 explains the lower average growth in the state of charge (SOC) throughout the winter.

1. During the summer, photovoltaic (PV) systems provide a larger percentage of the energy needed to meet the power demand.

2. In contrast, the ultracapacitor and Battery Energy Storage System (BESS) provide the bulk of the EV energy needed during the winter, when there is less availability of PV energy, lowering the battery's average state of charge.

By comparing the performance of hybrid energy storage sources with renewable sources managed by the Maximum Power Point Tracking prediction and optimization system with Conventional Renewable Energy Systems (RES), the usefulness of hybrid resources under the proposed structure is demonstrated. Load management is challenging because environmental factors have a significant impact on the amount of electricity produced by renewable energy sources like solar and wind. solar power generation.

6.5. Broader Implications for HEV Battery Lifespan and Performance

The proposed research carries significant implications for both the lifespan and performance of HEV batteries. By replacing traditional static SOC control with a dynamic, forecast-informed strategy, the system is able to minimize deep discharge cycles and avoid frequent high-rate charging/discharging events. These operating conditions are among the primary factors responsible for premature battery degradation. Consequently, the proposed method directly contributes to extending battery life, reducing replacement costs, and improving the overall sustainability of HEV systems.

From a performance standpoint, the integration of the ultracapacitor with the battery in a dynamically managed system enhances the ability to handle transient peak loads, such as rapid acceleration or regenerative braking, without placing undue stress on the battery. This ensures that the battery is primarily utilized for steady-state power delivery, while the ultracapacitor absorbs short-term fluctuations. Such an arrangement improves round-trip efficiency, reduces internal resistive heating, and maintains more stable SOC levels, which translates to higher reliability and consistent driving performance.

Moreover, by incorporating solar irradiance forecasts through ANN–HDKR modelling, the system achieves better synchronization between renewable generation and battery charging cycles. This proactive scheduling not only increases the fraction of renewable energy utilization but also reduces dependence on grid electricity or fossil-fuel-driven charging. Over time, this makes HEVs more environmentally friendly, while simultaneously improving their economic viability by lowering the cost of energy consumption.

In the broader context, the proposed methodology demonstrates how intelligent energy management strategies can transform HEVs from being only partial substitutes for fossil-fuel vehicles into highly optimized, renewable-energy-integrated systems. This represents a step toward climate-neutral mobility solutions, where both performance

and battery longevity are optimized without compromising user convenience.

7. Conclusion

This work proposed an integrated methodology to enhance solar irradiance forecasting and optimize energy management in battery–ultracapacitor hybrid electric vehicles (HEVs). The hybrid HDKR–ANN model delivered high forecasting accuracy (R^2 = 0.8818, RMSE = 0.269), confirming its effectiveness in estimating beam, diffuse, and reflected irradiance on tilted surfaces. This improved reliability strengthens PV utilization and provides a robust foundation for renewable energy integration in HEVs.

On the operational side, the proposed rule-based EMS with dynamic SOC control effectively coordinated energy flows between the PV system, battery, and ultracapacitor. Results demonstrated a 47.6% reduction in peak battery stress, extending battery lifespan while maintaining stable system performance across diverse driving and auxiliary load conditions. Seasonal analysis further revealed distinct operational behaviours: summer offered high PV generation and grid export but lower average SOC due to delayed charging, whereas winter imposed greater reliance on the battery and grid under reduced solar availability. Transitional periods exhibited more balanced profiles, highlighting the adaptability of the framework under varying conditions.

Overall, this study demonstrates that combining accurate solar forecasting with adaptive EMS strategies can significantly improve efficiency, storage durability, and renewable integration in HEVs.

Future directions include hardware-in-the-loop validation and reinforcement learning–based cost prediction, aiming to enhance real-time adaptability and economic feasibility in next-generation low-emission transportation systems.
feasibility.

Credit Authorship Contribution Statement

Shraddha Kaushik: Conceptualization, Data curation, Formal analysis, Investigation, Methodology, Software, Validation, Visualization, Writing - original draft, Writing - review & editing. **Kunamneni Rachanajali:** Formal analysis, Funding acquisition, Project administration, Resources, Supervision, Visualization, Writing - original draft, Writing - review & editing.

Declaration Of Competing Interest

The authors declare that they have no known competing financial interests or personal relationships that could have appeared to influence the work reported in this paper. The ethical issues; including plagiarism, informed consent, misconduct, data fabrication and/or falsification, double publication and/or submission, redundancy has been completely observed by the authors.

Funding

This research received no external funding.

Data Availability

Data collected for the study can be made available upon request from the corresponding author.

References

[1] A. Ghosh, “Possibilities and challenges for the inclusion of the Electric Vehicle (EV) to reduce the carbon footprint in the transport sector: A review,” *Energies*, vol. 13, no. 10, Art. no. 2602, 2020.

[2] J. Zhang, H. Sun, and B. Wang, “Solar irradiance prediction based on deep learning: A review,” *Renewable Sustainable Energy Rev*., vol. 122, Art. no. 110269, 2020.

[3] M. Guermoui and S. Benkaciali, “A novel ensemble learning approach for hourly global solar radiation forecasting,” *Neural Comput. Appl.*, 2022, vol. 34, no. 4, pp. 1–23, 2022.

[4] H. Romero and M. A. Gonzalez, “Applications of artificial intelligence to photovoltaic systems: A review,” *Appl. Sci.*, vol. 12, no. 19, Art. no. 10056, 2022.

[5] B. Benamrouq and M. Ouardouz, “A proposed model to forecast hourly global solar irradiation based on satellite-derived data, deep learning, and machine learning approaches, *J. Ecol. Eng.*, vol. 21, no. 4, pp. 26–38, 2020.

[6] A. F. Amiri and S. Kichou, “Fault detection and diagnosis of a photovoltaic system based on deep learning using CNN and Bi-GRU,” *Sustainability*, vol., no. 3, Art. no. 1012, 2024.

[7] D. T. Reindle, W. A. Beckman, and W. A. Duffie, “Diffuse fraction correlations,” *Sol. Energy*, vol. 45, no. 1, pp. 1–7, 1990.

[8] J. Bilbao, A. D. Miguel, and J. A. Franco, “Iso-Radiation maps for tilted surfaces in the Castile and Leon region, Spain,” *Energy Convers. Manag*., vol. 44, no. 9, pp. 1575–1588, 2003.

[9] A. Kudish and A. Ianetz, “Evaluation of the relative ability of three models to predict the global radiation on a tilted surface,” *Energy Convers. Manag.*, vol. 32, pp. 387–394, 1991.

[10] S. Yu, D. Lin, Z. Sun, "Efficient model predictive control for real-time energy optimization control of battery- ultracapacitor in electric vehicle," *International Journal Energy Resources*, vol. 44, pp. 7495-7506, 2020.

[11] P. J. Brockwell and R. A. Davism, “Introduction to time series and forecasting; Springer: Berlin/Heidelberg, Germany, 2002.

[12] S. I. Habib and S. A. G. K. Abadi, “A model predictive control strategy for performance improvement of hybrid energy storage systems in DC microgrids,” IEEE Access, vol. 10, pp. 25400–25421, 2022.

[13] M. Suhail, “Development of progress fuzzy logic and ANFIS control for energy management of plug-in

hybrid electric vehicle," *IEEE Access Open J.*, vol. 9, 2020.

[14] P. Kumar, R. P. Satish, S. Chandrasena, V. Ramu, G.N. Srinivas, K. Victor Sam Moses Babu, "Energy management system for small-scale hybrid wind solar battery-based microgrid," *IEEE Access*, vol. 8, pp. 8336–8345, 2020.

[15] J. Zhao, "An energy management strategy to reduce the comprehensive cost of hybrid energy storage systems in electric vehicles," *IEEE Access*, vol. 11, 2023.

[16] G. P. Zhang, "Time series forecasting using a hybrid ARIMA and neural network model, *Neurocomputing*, vol. 50, pp. 159–175, 2005.

[17] S. Sun and J. Zhang, "A Machine learning method for predicting driving range of battery electric vehicles," *J. Adv. Transp.*, pp. 1–16, 2016.

[18] M. Al-Shamisi, A. Assi, and H. Hejase, "Estimation of global solar radiation using artificial neural networks in Abu Dhabi City, UAE," *J. Sol. Energy Eng.*, vol. 136, no. 2, Art, no. 024502, 2014.

[19] A. Rahimikhoob, "Estimating global solar radiation using artificial neural network and air temperature data in a semi-arid environment," *Renew. Energy*, vol. 35, no. 9, pp. 2131–2135, 2010.

[20] W. Zhou, W. Wang, X. Hua, and Y. Zhang, "Real-time traffic flow forecasting via a novel method combining periodic-trend decomposition," *Sustainability-Basel*, vol. 12, no. 15, Art. no. 5891, 2020.

[21] J. E. Hay, J. A. Davies, "Calculations of the solar radiation incident on an inclined surface," *Sol. Energy*, , vol. 24, no. 5, pp. 429–431, 1980.

[22] K. P. T. T. L. N. Ding, "Design of a hybrid energy management system using rule-based control strategy and genetic algorithm for the series-parallel plug-in hybrid electric vehicle," *Int. J. Energy Res.*, vol. 45, no. 2, pp. 1627–1644, 2020.

[23] K. Prasada and N. Ding, "Design of a hybrid energy management system using rule-based control strategy and genetic algorithm for the series-parallel plug-in hybrid electric vehicle," *Int. J. Energy Res.*, vol. 45, no. 2, pp. 1627–1644, 2020.

[24] D. Fischer and H. Madani, "On heat pumps in smart grids: A review," *Renew. Sustain. Energy Rev.*, 70, pp. 342–357, 2017.

[25] A. Ghorashi and S. I. Habibi, "A model predictive control strategy for performance improvement of hybrid energy storage systems in DC microgrids," *IEEE Access*, vol. 10, pp. 25400–25421, 2022.

[26] N. Patel and R. Sharma, "Advanced photovoltaic energy forecasting using deep neural networks," *Renew. Energy*, vol. 208, pp. 1253–1265, 2023.

[27] H. A. Trinh, "Optimization-based energy management strategies for hybrid construction machinery: A review," *Energy Reports*, vol. 8, pp. 6035–6057, 2022.

[28] Y. Zheng and X. Luo, "Seasonal solar irradiance forecasting using artificial intelligence," *Sci. Rep.*, vol. 14, Art. no. 68531, 2024.

[29] A. Kumar and S. Mehta, "Hybrid machine learning and optimization method for solar irradiance prediction," *Eng. Optim.*, vol. 56, no.2, Art. no. 2390126, 2024.

[30] M. Rahman and T. Singh, "Optimizing hardware configuration for solar-powered energy management in battery-ultracapacitor hybrid electric vehicles," *Sci. Rep.*, vol. 14, Art. no. 80219, 2024.

[31] H. Zhang and L. Li, "A Hybrid ensemble model for solar irradiance forecasting," *Electronics*, vol. 12, no. 12, Art. no. 2607, 2023.

[32] J. Baker and S. Das, "Sustainable power management in light electric vehicles with hybrid energy storage systems," *Sci. Rep.*, vol. 14, Art. no. 10920784, 2024.

[33] F. Ali and R. Hasan, "AI-Based Forecasting for optimized solar energy management and smart grid reliability," *Int. J. Prod. Res.*, vol. 61, no. 5, Art. no. 2269565, 2023.

[34] M. Santos and G. Chang, "Systematic review on impact of different irradiance forecasting models on solar energy systems," Energies, vol. 15, no. 17, Art. no. 6267, 2022.

[35] D. Lee and C. Wang, "A renewable approach to electric vehicle charging through solar integration," *Sci. Rep.*, *vol.* 14, Art. no. 10903804, 2024.

[36] I. A. Hassanvand, J. Ebrahimi, and M. Abasi, "Voltage regulation in low voltage distribution networks using reactive power capability of photovoltaic inverters and PID consensus algorithm," *Journal of Applied Research in Electrical Engineering*, vol. 3, no. 2, pp. 159–167, 2024.

[37] A. Rahmani, M. Dehghani, and S. M. Rezaee, "Optimal energy management scheduling for hybrid electric vehicles using deep neural network-based control of battery–ultracapacitor hybrid storage systems," *Journal of Applied Research in Electrical Engineering*, vol. 4, no. 2, pp. 85–96, 2023.

[38] J.E. Hay and J.A. Davies, "Calculations of the solar radiation incident on an inclined surface," *Solar Energy*, vol. 24, no. 5, pp. 429–435, 1980.

[39] D. T. Reindle, W. A. Beckman, and W. A. Duffie, "Diffuse fraction correlations," *Sol. Energy*, vol. 45, no. 1, pp. 1–7, 1990.

[40] J. A. Duffie and W. A. Beckman, *Solar Engineering of Thermal Processes*, 4th ed., Wiley, 2013.

[41] M. Iqbal, *An Introduction to Solar Radiation*, Academic Press, 1983.



Shraddha Kaushik received his bachelor of Electrical and Electronics Engineering from Government Engineering College Raipur, India in 2009. She has completed her Master's in Engineering (Power Systems & Automation) from GITAM University, Vishakhapatnam, India. She is currently pursuing her Ph.D. Degree from Vignan Foundation for Science Technology & Research, Guntur, India. Currently, she is serving as an Assistant Professor at the Bhilai Institute of Technology in Durg, India. She has 10 years of teaching experience in Electrical Engineering courses in both undergraduate and postgraduate. She has supervised 6 ME scholar theses and published 21 articles in peer-reviewed journals and conferences. Her current research includes Power Converters, active filtering, power conditioning, machine learning, AI, power system analysis &Electric Vehicles.



Kunamneni Rachanajali received his bachelor of Electrical and Electronics Engineering from JNTU Kakinada (Vignan's Engineering College, Guntur, AP)In 2011. She completed her Master's in Engineering from Visvesvaraya National Institute of Technology, Nagpur (VNIT Nagpur) In 2013. She obtained Ph.D. Degree from Vignan's Foundation for Science Technology & Research, Guntur, India in 2021. Currently, she is serving as an Assistant Professor in the Department of Electrical and Electronics Engineering at Vignan's Foundation for Science, Technology & Research (Deemed to be University). She has 10 years of teaching experience in Electrical Engineering courses both undergraduate and postgraduate. She has supervised 10 ME scholar theses and published 30 articles in peer-reviewed journals and conferences. Her current research includes Power Converters, active filtering, power conditioning, power electronics, AC and DC drives, and High Voltage Engineering.

Copyrights
© 2026 Licensee Shahid Chamran University of Ahvaz, Ahvaz, Iran. This article is an open-access article distributed under the terms and conditions of the Creative Commons Attribution –NonCommercial 4.0 International (CC BY-NC 4.0) License (http://creativecommons.org/licenses/by-nc/4.0/).